Proceedings of the 2nd International Conference on Functional Materials and Civil Engineering
DOI: 10.54254/2755-2721/98/20241121

Influence of Water Ingress at the Shield Tunnel Portal on Tunnel Deformation and Load Capacity Weakening

Yongliang Huang[1,2,3,4], Hu Li[1,2,3,5], Xiaofei Ye[1,2,3], Kai Wang[1,2,3]

[1]Jinan Rail Transit Group Co., Ltd., Jinan, Shandong, 250014, China;
[2]Shandong Rail Transit Intelligent Construction and Operation Technology Engineering Research Center, Jinan, Shandong, 250014, China;
[3]Shandong Key Laboratory of Intelligent Rail Transit Information and Equipment, Jinan, Shandong, 250014, China;
[4]Shandong Rail Transit Research Institute Co., Ltd., Jinan, Shandong, 250014, China

[5]793231271@qq.com

Abstract. During the construction of shield tunnels, adverse geological conditions can lead to tunnel segment settlement and damage. This study investigates the deformation patterns and changes in load capacity of shield tunnels under water ingress conditions at the portal, using a segment of the Jinan Metro as a case study. Through field measurements and numerical simulations, we analyzed the structural deformation and weakening of load capacity caused by water ingress. The results indicate that significant settlement occurs at both the tunnel crown and invert after water ingress, with a maximum settlement of 181.2 mm compared to the original design axis. The deformation profile of the tunnel primarily resembles a transverse "duck egg" shape, while the segments near the portal exhibit vertical "duck egg" deformations due to grouting and other factors. Multiple cracks and damages were observed in the segments, with up to 16 cracks found in a single ring. Compared to the original design conditions, the bending moment in the tunnel lining increased by approximately 7%, and the axial force increased by about 9%, leading to an 11% reduction in tunnel resistance effects. The findings of this study regarding tunnel lining deformation and load capacity weakening provide valuable insights for similar engineering projects.

Keywords: Shield Segment, Damage Detection, Deformation Patterns, Load Characteristics.

1. Introduction

Common methods for subway tunnel construction include the mining method and the shield method. Among these, the shield method is widely used in urban subway construction due to its high safety and efficiency. However, tunnels face various issues such as deformation during construction and operation periods [1-2]. The differences in geological conditions and groundwater distribution can pose safety risks during shield construction. Common remedial measures include grouting inside the tunnel and at the surface to block the infiltration paths of water flow, thereby reducing the permeability of the soil and isolating groundwater from the tunnel structure [3-4]. The changes in load capacity of the tunnel segments after grouting are critical for the stability of the tunnel [5]. The risks during the shield tunnel construction phase are primarily concentrated at the launch and reception stages. Water and sand ingress

DOI: 10.54254/2755-2721/98/20241121

can lead to surface subsidence, and the collapse of the overlying soil can cause deformation in the tunnel structure, resulting in segment deformation and leakage issues. Research by Ding Wenqi et al. [6] investigated the impact of misalignment on the bending mechanics of shield segment longitudinal seams, while Cao Songyu et al. [7] studied the influence of crack locations on the structural damage of shield tunnel segments. A considerable amount of research has been conducted on the changes in load characteristics due to tunnel damage and crack factors [7-12]. However, there is limited research specifically focused on the deformation patterns and load capacity weakening caused by water ingress during the initial stage of tunnel construction, indicating a need for further investigation.

This study focuses on the shield tunnel at Xiangyang Station on Line 3 in Jinan, Shandong Province. Through field measurements, we investigate the deformation patterns of the tunnel and utilize numerical simulations to reveal the characteristics of changes in load capacity, providing valuable insights for similar engineering projects.

2. Engineering Background

2.1. Geological Overview

The Jinan urban rail transit segment spans a length of 3,516 meters and utilizes a single circular shield tunnel. The geological layers exposed along the route can be categorized based on their sedimentary age and engineering properties, including artificial fill, Quaternary silty clay, silt, and gravelly soil, with occasional exposures of cemented gravel lenses. The tunnel is buried at depths ranging from 10.1 to 14.5 meters. This section lies within the runoff area from the Yellow River to the Xiaoqing River, where groundwater is primarily found in the silty clay, silt, and gravelly soil layers. The groundwater type is mainly phreatic, with water levels varying between 1.70 to 8.00 meters deep, and stable water level elevations between 16.15 to 16.56 meters.

2.2. Tunnel Lining Design

The tunnel features a circular lining constructed from a single-layer reinforced concrete prefabricated structure. The internal diameter of the segments is 5,800 mm, the external diameter is 6,400 mm, and the thickness is 300 mm, with a ring width of 1,200 mm. Each lining ring consists of one crown block (K), two adjacent blocks (B), and three standard blocks (A). The wedge-shaped lining ring is designed as a double-sided wedge with a wedge height of $\Delta = 48.00$ mm and a wedge angle of $\beta = 0.43°$. The concrete strength is rated at C50, and the impermeability level is P12. The structural cross-section of the tunnel segments is shown in Figure 1. The lining ring is composed of six sections: three standard blocks (with a central angle of 67.5° each), two adjacent blocks (also with a central angle of 67.5°), and one crown block (with a central angle of 22.5°). The joints of the lining rings are connected using bent bolts, with 16 M27 bolts for the ring joints and 12 M27 bolts for the longitudinal joints. The assembly of the lining rings employs a staggered joint arrangement.

3. Analysis of Tunnel Deformation

3.1. Incident Process

The water inflow event occurred at the left line tunnel entrance of the vertical shaft for the shield tunneling. After completing the assembly of the 11th ring, the muck discharge noticeably decreased at the screw muck outlet. Following the completion of the 14th ring assembly, a small amount of water and mud emerged beneath the curtain pressing plate. During the secondary grouting process to seal the tunnel entrance, personnel noticed a sudden increase in water and mud inflow. Inspectors discovered cracks on the ground surface. In response, relevant units promptly implemented emergency measures, including external grouting (bentonite and shield tail grease), internal grouting (two-component grout, polyurethane, and chemical grout), sandbag counterpressure at the tunnel entrance, and groundwater lowering. After emergency treatment, the tunnel entrance showed no leakage, indicating effective sealing.

DOI: 10.54254/2755-2721/98/20241121

3.2. Tunnel Deformation Analysis

Following the emergency response, elevation measurements of the tunnel's crown were conducted in the 0-20 ring detection area, with results shown in Figure 1. The measurements revealed that the crown elevations of rings 1-20 experienced settlement compared to the design elevations. The lowest point of settlement was at ring 15, with an actual absolute elevation of 2.2909 m compared to a design elevation of 2.4551 m, representing a relative drop of 164.2 mm. Similarly, the crown elevation also exhibited settlement, with rings 1-3 and 6-20 experiencing reductions. The lowest crown elevation was again at ring 15, measured at 8.0739 m against a design height of 8.2551 m, resulting in a relative decrease of 181.2 mm.

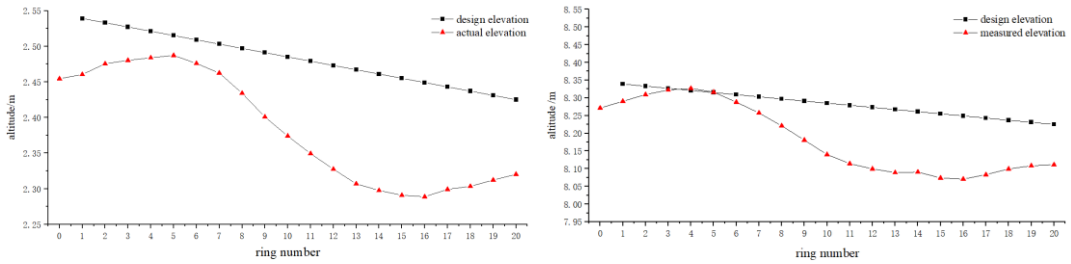

(a) Crown Elevation Measurement (b) Base Elevation Measurement

Figure 1. Longitudinal Section Deformation

For the 0-20 ring segments, cross-sectional scanning was conducted, with results illustrated in Figure 2. The scan data revealed that rings 0-6 exhibited vertical egg-shaped deformation, with the vertical axis elongated. The maximum deformation reached 4.4 cm at ring 3, and the maximum ellipticity was 14.31‰ at ring 4. In contrast, rings 7-20 displayed horizontal egg-shaped deformation, with the horizontal axis elongated. Both the maximum deformation and ellipticity for these rings were recorded at ring 11, measuring 4.0 cm and 13.28‰, respectively.

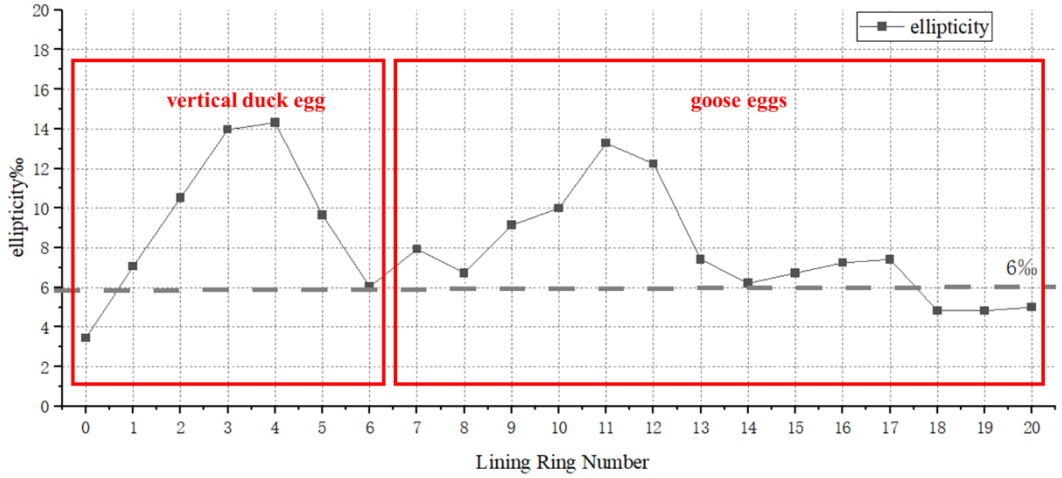

Figure 2. Tunnel Ellipticity

3.3. Segment Damage Analysis

An inspection of the tunnel segments revealed damage in a total of 21 rings, with 17 rings showing cracks. In total, 151 cracks were detected, as illustrated in Figure 3. The cracks primarily occurred at the sides and the crown of the segments, predominantly displaying a longitudinal distribution, with several cracks extending along the length of the segments. Eleven rings exhibited more than five cracks, while eight rings had over ten cracks, specifically in rings 1-5, 8-9, and 18.

DOI: 10.54254/2755-2721/98/20241121

ring number	0	1	2	3	4	5	6	7	8	9	10	11	12	15	16	17	18
Number of cracks	5	11	12	15	12	14	10	9	16	16	1	6	5	2	3	3	11

Figure 3. Crack Development Concentration Diagram

All segments in ring 20 displayed damage, with a total of 149 identified instances of damage. The area of damage for each segment is depicted in Figure 4, totaling 15.2095 m². The damage was concentrated at the ring and longitudinal seams, with 91% occurring at the ring seams, often near longitudinal bolts. The largest damaged area measured 140 cm by 50 cm, found at the B2 segment seam of ring 2. Among the 149 instances of damage, 51 were classified as non-delaminated, while 45 were delaminated. Ring 9 exhibited the greatest total damage area, with 18 instances of damage totaling 2.3148 m².

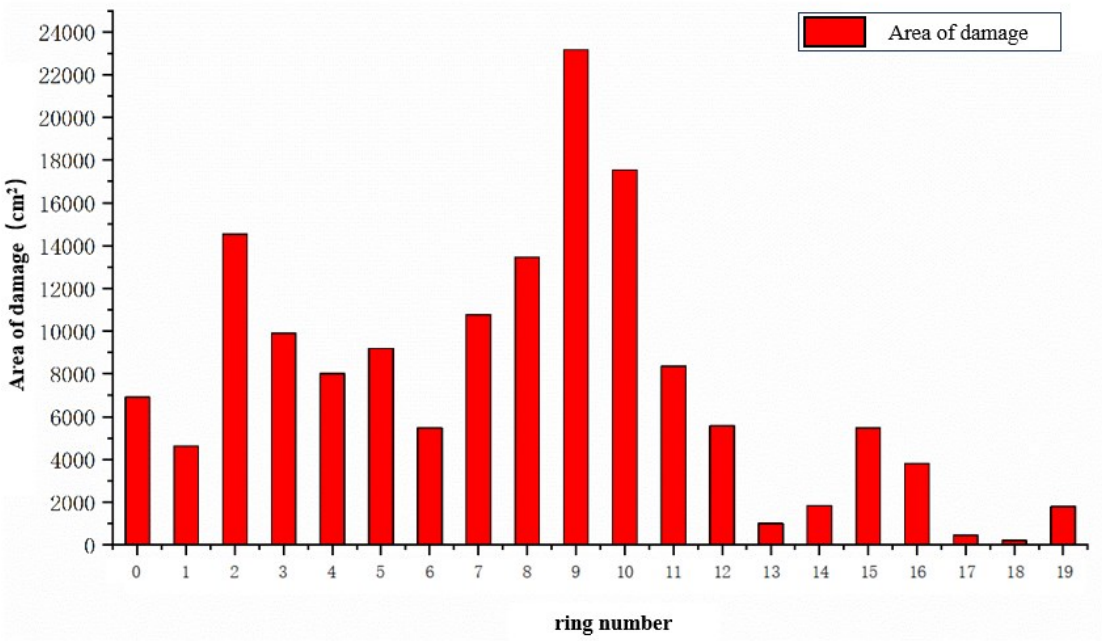

Figure 4. Damage Area Distribution Diagram

4. Analysis of Load Capacity Weakening

4.1. Condition Settings

After the tunnel lining is damaged, the safety of the tunnel structure is compromised. To accurately determine the weakening pattern of the tunnel's load-bearing capacity, a comparative study of the original construction conditions and the current conditions was conducted using numerical simulations. This method helps reveal the changes in the tunnel's load-bearing performance.

The conventional calculation theory adopts the homogeneous ring method, treating the circular tunnel lining structure composed of **n** segments as a homogeneous ring body with uniform stiffness. Considering the existence of segment joints, the bending stiffness of the entire ring is multiplied by a stiffness reduction factor η, which accounts for the reduced stiffness at the joints. The internal force distribution in the ring is then obtained under the combined action of load and ground resistance. When considering the staggered joint assembly effect, the bending moment on the segments increases relative

DOI: 10.54254/2755-2721/98/20241121

to the joints under co-deformation conditions. Therefore, the bending moment of the homogeneous ring is multiplied by a bending moment increase factor (1+ξ) for the segments, while the bending moment at the joints is multiplied by a bending moment reduction factor (1−ξ), resulting in the corrected bending moment distribution.

According to subway design specifications, the water and earth pressures are calculated separately. The ground overload is set at 20 kPa, the self-weight of the structure at 8.75 kPa, the vertical soil pressure on the top at 202.3 kPa, the backfill soil pressure P_i at 31.3 kN/m, the lateral soil pressure at the top P_1 at 77.3 kPa, the lateral soil pressure at the bottom P_2 at 96.1 kPa, the ground reaction P_r at 209.2 kPa, and the water pressure at the bottom P_2 at 196.5 kPa. ccording to the construction plan, the shield tunneling method involves simultaneous grouting during excavation. The shield machine's built-in synchronous grouting system performs four-point grouting. The grouting load is modeled as a triangular load with a maximum value of 500 kPa, and the grouting points are located at 22.5°, 112.5°, 202.5°, and 292.5°. In the original design construction condition, material strengths are selected based on design values: the design compressive strength of concrete is fc=23.1N/mm^2, the tensile strength is ft=1.89N/mm2, and the elastic modulus is Ec=3.45×104N/mm^2. The steel reinforcement has a yield strength fy=fy'=360 N/mm^2 and an elastic modulus of Ec=2.0×105N/mm^2。

The current condition analysis uses a shell-spring model, which was established using the ANSYS software. The model schematic is shown in Figure 7. The lining structure was created based on the actual design dimensions: a ring width of 1.2 m, segment thickness of 0.35 m, and a calculated radius of 2.925 m. The segmentation and assembly angles were kept identical to the actual structure, including one crown segment (F, 20°), two adjacent segments (L, 68.75°), and three standard segments (B, 67.5°). Nonlinear shell elements were used to simulate the segments. The longitudinal and circumferential joints were simulated with spring elements, accounting for the concrete compression, radial and longitudinal shear effects at the joint locations, and the nonlinear behavior of the bolts, as shown in Figure 5(b).

For the current condition analysis, the displacement-structure method was used to back-calculate the internal forces of the lining structure based on the measured data. The bending moments and axial forces at the segment and joint locations of the lining structure were calculated under the current deformation state by back-calculating from the on-site measured convergent deformation data. Using the measured offsets between rings, forced displacement was applied to the ring joints in the model to back-calculate the shear forces at the ring joints. The safety of the lining structure under current and future conditions was assessed based on the internal forces within and between the lining rings. During the calculations, a multi-ring model was established to compute both the forces at the ring joints and the internal forces of the lining rings.

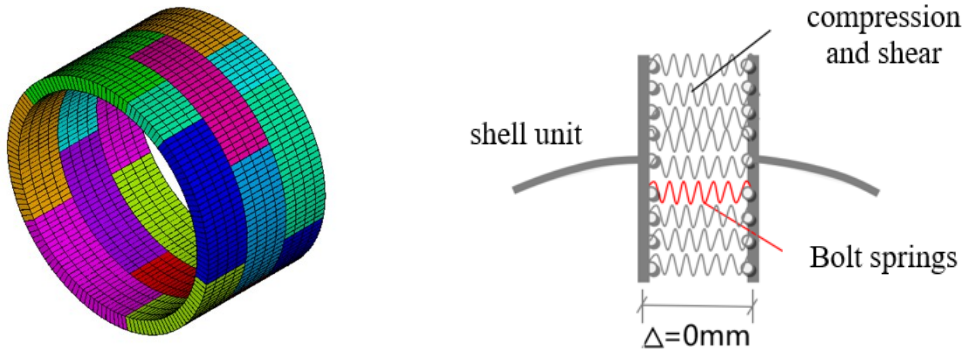

(a) Lining Structure Model (b) Segment Joint Model

Figure 5. Model Diagram

DOI: 10.54254/2755-2721/98/20241121

4.2. Calculation Results

The bending moment and axial force diagrams generated using ANSYS software are shown in Figure 6 (calculated per meter in the software, with a check considering a ring width of 1.2 m).

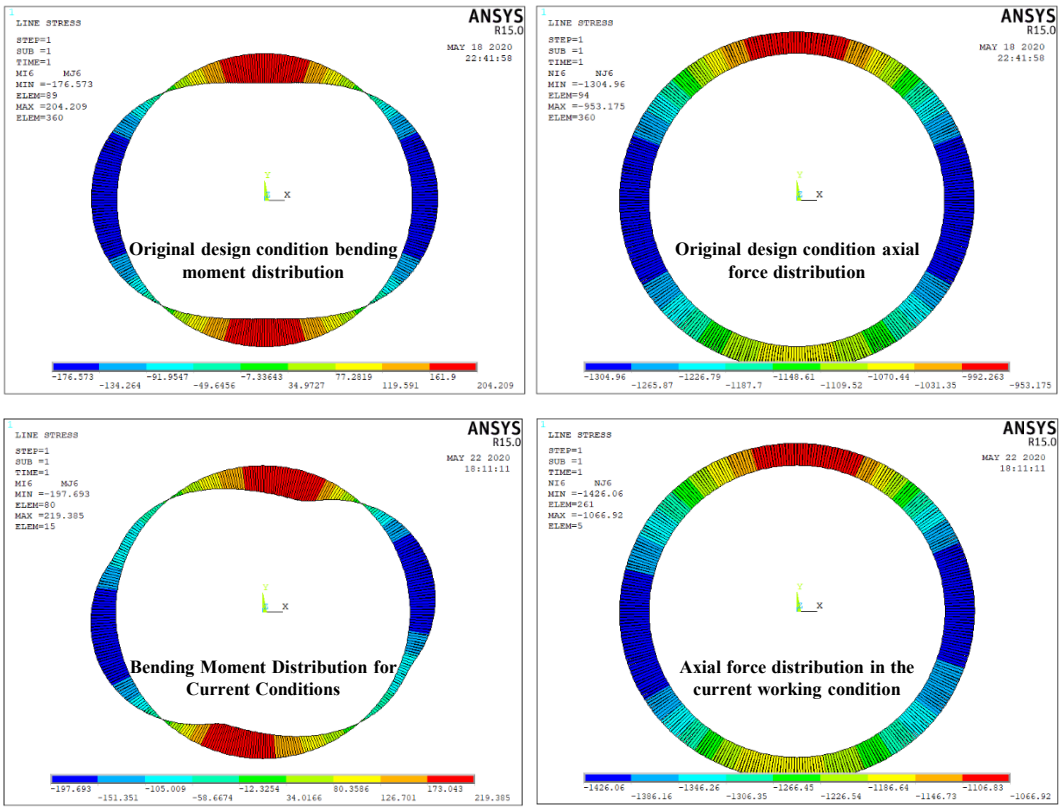

Figure 6. Bending Moment and Axial Force Calculation Results Under Different Conditions

Taking the 8th ring of the left tunnel line as an example, we collected the bending moments and axial forces for each lining ring under both the original design condition and the current condition. From the diagram, it can be observed that, under the original design condition, the maximum positive bending moment occurred in segment B1, with a maximum value of 204 kN·m. The calculated bending capacity at this location is 329 kN·m. The maximum negative bending moment occurred in segment F, with a maximum value of -176 kN·m. The calculated bending capacity at this location is -345 kN·m. The maximum axial force was found in segment B3, with a value of 1304 kN, and the calculated compressive capacity at this location is 8490 kN. The resistance effect ratio R/S was calculated, with the minimum value being 1.61.

Under the current condition, the maximum positive bending moment occurred in segment B1, with a maximum value of 219 kN·m. The calculated bending capacity at this location is 316 kN·m. The maximum negative bending moment occurred in segment F, with a maximum value of -197 kN·m. The calculated bending capacity at this location is -365 kN·m. The maximum axial force was found in segment B3, with a value of 1426 kN, and the calculated compressive capacity at this location is 7980 kN. The resistance effect ratio R/S was calculated, with the minimum value being 1.44.

The comparative analysis shows that the water inflow caused deformation in the tunnel structure, increasing the internal forces. Compared to the original design condition, the bending moment increased by approximately 7%, the axial force increased by approximately 9%, and the minimum resistance effect ratio decreased by about 11%. However, under the current condition, the tunnel still meets the load-bearing capacity requirements.

DOI: 10.54254/2755-2721/98/20241121

5. Conclusion

Based on the damaged tunnel segment project of a certain shield tunnel section in the Jinan Metro, this paper analyzes the deformation patterns and load-bearing capacity changes of the damaged shield tunnel through on-site inspections and numerical simulations. The following conclusions were drawn:

(1) The deformation characteristics of the shield tunnel were inspected and analyzed, revealing settlement at both the tunnel invert and portions of the tunnel crown, with relative subsidence ranging between 160 mm and 180 mm. An analysis of the tunnel's ovality showed that 30% of the segments exhibited vertical "duck egg" deformation, while 70% showed horizontal "duck egg" deformation. Among the 21 rings, 17 rings displayed cracking issues, indicating a damage rate of 80%, with water ingress significantly affecting tunnel deformation and damage.

(2) Numerical simulations were conducted to compare the original design conditions and the current deformed state. The results indicate that after deformation, the internal forces within the tunnel structure increased, leading to an approximate 11% reduction in load-bearing capacity. Despite this reduction, the post-deformation load-bearing capacity still meets the necessary requirements. Reinforcement measures such as installing steel rings or applying carbon fiber plates can be used to further enhance the structure's load-bearing capacity.

References

[1] He, C., Feng, K., & Fang, Y. (2015). Current status and prospects of shield tunneling technology in subway tunnel construction. Journal of Southwest Jiaotong University, 50(01), 97-109.

[2] Ge, S., Gao, W., Wang, Y., et al. (2023). A review of diseases, evaluation, and treatment of transportation shield tunnels in China. China Civil Engineering Journal, 56(01), 119-128. DOI: 10.15951/j.tmgcxb.21111120.

[3] Ye, F., Zhu, H., & He, C. (2009). Grouting diffusion mode and pressure analysis on segments in shield tunnel construction. Rock and Soil Mechanics, 30(05), 1307-1312. DOI:10.16285/j.rsm. 2009.05.011.

[4] Liu, W., Zhao, T., Zhang, Y., et al. (2017). Analysis of safety risk patterns and countermeasures in shield construction for subway. China Safety Science Journal, 27(10), 130-136.DOI:10. 16265/j.cnki.issn1003-3033.2017.10.022.

[5] Lai, J., Qiu, J., Pan, Y., et al. (2015). Comprehensive monitoring and analysis of segment cracks in shield tunnels. Modern Tunneling Technology, 52(02), 186-191. DOI:10.13807/j.cnki.mtt. 2015.02.028.

[6] Ding, W., Wu, Y., Zhang, X., et al. (2023). Influence of staggered joints on the mechanical behavior of longitudinal seams in shield tunnel segments. China Journal of Highway and Transport, 36(11), 256-265. DOI:10.19721/j.cnki.1001-7372.2023.11.007.

[7] Cao, S., Wang, S., Liu, C., et al. (2020). Influence of crack position on structural failure modes of shield tunnel segments. Journal of Southeast University (Natural Science Edition), 50(01), 120-128.

[8] Zhang, L., Feng, K., Liang, X., et al. (2023). Study on evaluation methods for bearing capacity of shield tunnel segments. Journal of Tongji University (Natural Science Edition), 51(09), 1334-1343.

[9] Gao, X., Li, P., Zhang, M., et al. (2023). Bearing characteristics and failure mechanism of partially failed shield tunnel segments. China Journal of Highway and Transport, 36(11), 302-311. DOI: 10.19721/j.cnki.1001-7372.2023.11.011.

[10] Zhang, Y., Liu, T., Zhu, C., et al. (2023). Model test study on deformation and failure characteristics of shield tunnels in soil-rock composite strata under overload. Journal of Railway Science and Engineering, 20(11), 4277-4287. DOI:10.19713/j.cnki.43-1423/u. t20222174.

[11] Yuan, Q. (2022). Analysis of deformation and bearing performance of shield tunnels in soft soil considering nonlinearity of segment joints (Master's thesis). Tongji University. DOI:10. 27372/d.cnki.gtjsu.2022.000768.

DOI: 10.54254/2755-2721/98/20241121

[12] Liu, X., Zhang, Y., & Wang, R. (2020). Discussion on deformation and failure of lining structure of subway shield tunnels. China Civil Engineering Journal, 53(05), 118-128. DOI:10.15951/j.tmgcxb.2020.05.008.